

## Article

# Formation of Complex Inclusions in Gear Steels for Modification of Manganese Sulphide

Haseeb Ahmad <sup>1</sup>, Baojun Zhao <sup>2,\*</sup>, Sha Lyu <sup>3,\*</sup>, Zongze Huang <sup>4</sup>, Yingtie Xu <sup>4</sup>, Sixin Zhao <sup>4</sup> and Xiaodong Ma <sup>1,\*</sup>

<sup>1</sup> Sustainable Minerals Institute, The University of Queensland, Brisbane 4072, Australia; h.ahmad@uq.edu.au

<sup>2</sup> REEM International Institute for Innovation, Jiangxi University of Science and Technology, Ganzhou 341000, China

<sup>3</sup> Department of Materials Science and Engineering, Southern University of Science and Technology, Shenzhen 518055, China

<sup>4</sup> Baoshan Iron and Steel Co., Ltd., Shanghai 200122, China; zzhuang@baosteel.com (Z.H.); xuyingtie@baosteel.com (Y.X.); zhaosixin@baosteel.com (S.Z.)

\* Correspondence: bzhan@jxust.edu.cn (B.Z.); lus@sustech.edu.cn (S.L.); x.ma@uq.edu.au (X.M.)

**Abstract:** Suitable MnS inclusions in gear steel can significantly improve the steel machinability and reduce the manufacturing costs. Two gear steel samples with different sulphur contents were prepared via aluminium deoxidation followed by calcium treatment. The shape, size, composition and percentage distribution of the inclusions present in the steel samples were analyzed using an electron probe micro-analysis (EPMA) technique. The average diameter of MnS precipitated on an oxide inclusion is less than 5  $\mu\text{m}$ . It was found that the steel with high sulphur content contains a greater number of elongated MnS precipitates than low sulphur steel. Moreover, there are more oxide inclusions such as calcium-aluminates and spinels with a small amount of solid solution of  $(\text{Ca},\text{Mn})\text{S}$  in low content sulphur steel after calcium treatment, which indicates the modification of solid alumina inclusions into liquid aluminates. The typical inclusions generated in high sulphur steel are sulphide encapsulating oxide inclusions and some core oxides were observed as spinel. The formation mechanisms of complex inclusions with different sulphur and calcium contents are discussed. The results are in good agreement with thermodynamic calculations.

**Keywords:** gear steel; inclusions characteristics; EPMA; sulphide modification



**Citation:** Ahmad, H.; Zhao, B.; Lyu, S.; Huang, Z.; Xu, Y.; Zhao, S.; Ma, X. Formation of Complex Inclusions in Gear Steels for Modification of Manganese Sulphide. *Metals* **2021**, *11*, 2051. <https://doi.org/10.3390/met11122051>

Academic Editor: Eli Aghion

Received: 4 November 2021

Accepted: 16 December 2021

Published: 18 December 2021

**Publisher's Note:** MDPI stays neutral with regard to jurisdictional claims in published maps and institutional affiliations.



**Copyright:** © 2021 by the authors. Licensee MDPI, Basel, Switzerland. This article is an open access article distributed under the terms and conditions of the Creative Commons Attribution (CC BY) license (<https://creativecommons.org/licenses/by/4.0/>).

## 1. Introduction

Gears structure a fundamental part in the running of different machines and cars for transmitting power. There are a range of gears used in different areas according to the particular prerequisites, such as automotive gears, mining gears, marine gears, wind turbines, bicycle gears, instrumentation gears and conveyor systems. The automotive industry requires automotive gears for high force capacity, high fatigue strength and to convert mechanical energy efficiently and silently. However, machining of gear steels, generally, is linked with high energy consumption and decreased cutting tool life. The worsening of mechanical properties depends on the amount, size, morphology and dispersion of non-metallic inclusions. Since the machining costs (estimated ~40%) represent a large fraction of the total production expenses of most components, considerable attention has been paid to designing innovative techniques and technologies that make machinability viable with mechanical properties [1–3]. Adding a small amount of sulphur (typically from 100 to 500 ppm) is known to cause an outstanding improvement in the machinability of gear steels via manganese sulphide formation, which improves the machinability via chip embrittlement and increases tool life. Sulphides, especially MnS, with a round or shaft morphology are usually advantageous for this purpose. MnS inclusions have good ductility and can easily bend into long strip shapes after hot working, which causes anisotropy [4] in steel properties, consequently reducing the fatigue life [3] and altering

the transverse properties of steel, and is furthermore destructive to the machinability of steels [5]. Most of the oxide and sulphide inclusions are endogenous, formed as the result of deoxidation of steel. However, dual phase types with or without sulphides and pure sulphide inclusions are generated during all succeeding stages of steel processing, even during solidification [1,6–10]. In contrast, alumina ( $\text{Al}_2\text{O}_3$ ) is another type of inclusion generated as the result of Al deoxidation in molten steel. Large and irregular shapes of alumina inclusions mostly float up towards the slag, while smaller alumina inclusions (less than 10  $\mu\text{m}$ ) unable to float up get stuck in the steel and solidify, which can act as a stress raiser or become a crack source or even help the crack propagation under cyclic loading, and suppress the anti-fatigue property of steel. In addition, too much  $\text{Al}_2\text{O}_3$  inclusions can cause nozzle clogging due to accumulation in the nozzle during the casting process, and because it is hard and brittle, it causes excessive tool wear in the machining process [7].

Normally, calcium addition is an effective way to alter the morphology and dispersion of non-metallic inclusions in the continuous casting process or in ingots. Calcium treatment is normally applied in Al-deoxidized steels to alter the solid alumina inclusions into liquid ones [11–13] which effortlessly pass through without spout impediment. In the current operations, the inclusions modification proficiency using Ca is usually not high; the surplus Ca may cause the development of high temperature stable inclusions such as  $\text{CaS}$  and  $\text{Ca}\cdot\text{Al}_{12}\text{O}_{19}$ , leading to spout impediment [2,10,14]. In resulphurized steel, Ca is also used to transform the  $\text{MnS}$  inclusions by reducing the relative plasticity of  $\text{MnS}$  inclusions during hot working. Blais et al. proposed the optimum Ca/S ratio to be 0.7 for effective modification of sulphide inclusions [15]. The reaction formation of  $\text{CaS}$  was reported via the formation of a  $\text{CaS}$  transient phase right after the Ca injection treatment [16] or formed after modification of  $\text{Al}_2\text{O}_3$  to calcium aluminates [17]. Verma et al. proposed that transit  $\text{CaS}$  can react with the alumina to yield modified inclusions [18,19], while Wang et al. proposed that the reaction between  $\text{Al}_2\text{O}_3\text{-CaO}$  inclusions with the dissolved [S] and [Al] in the melt forms  $\text{CaS}$  around the inclusions [20]. Park et al. studied the mechanism of complex inclusions formation by using synthetic slag without adding Ca in the melt and predicted the critical sulphur [S] level required to precipitate  $\text{CaS}$  in the inclusions. By increasing the  $\text{SiO}_2$  in the slag, the critical [S] level increases at a given [Al] content [21].

For uniform distribution of fine  $\text{MnS}$  precipitates, it is effective to use such oxides which have a high sulphide capacity and low melting temperature [11–13,22]. Miki [23] concluded that sulphur solubility in the inclusions increases with increasing  $\text{MnO}$  content in oxides, therefore increasing the probability of  $\text{MnS}$  precipitation on oxides. Thus, improvement of steel properties lies in the proper morphology control of oxides and sulphides. If the adverse effects of both sulphides ( $\text{MnS}$ ) and pure oxides ( $\text{Al}_2\text{O}_3$ ) can be minimized or even avoided via Ca treatment, the deformation of pure  $\text{MnS}$  precipitates will be easily confined, and also the oxide inclusions will not directly become the reason for steel failure. Although there is enough literature available on inclusions modification in Al-deoxidized and Ca-treated steels in lab scale models, there is very limited data available to improve the quality of industrial products because of the complex nature of reactions taking place in the ladle. To clearly define the role of Ca in modifying the sulphide and oxide inclusions in Al-killed Ca-treated gear steels, it is necessary to obtain the fundamental knowledge to understand the formation mechanism of inclusions including the composition of each phase from the viewpoint of thermodynamics and evolution during the steelmaking process on an industrial scale. Therefore, in this study we focused on the characterization and formation of complex oxide-sulphide inclusions in different sulphur-level industrial samples with an Al-deoxidation and Ca-treatment process. The formation mechanisms and thermodynamic prediction are discussed for the optimization of manganese sulphide modification.

## 2. Materials and Methods

To investigate the effect of sulphur and calcium on complex oxide and sulphide inclusions, two samples having different amounts of sulphur and calcium were taken from two industrial products. The chemical compositions of the samples are given in Table 1

below. Two steel grades (named GS1 and GS2) have almost the same Mn concentration: GS1 contains 290 ppm S and 14 ppm Ca, whereas GS2 contains 140 ppm S and 19 ppm Ca. The steelmaking process followed sequential steps through an electric arc furnace (EAF) → ladle (LF) refining → vacuum degassing (VD) → continuous casting (CC). Both samples underwent the same manufacturing route, i.e., the scrap metal along with hot metal from the converter was added into the electric arc furnace (Danieli & Co., Buttrio, Italy). During melting, oxygen lancing was used to reduce the carbon content to the desired level. After melting, the molten steel was tapped to the ladle furnace for further treatment, in which lumps of pure aluminum were added to reduce the oxygen content. Pure argon gas purging from the bottom was also employed to accelerate the mixing of aluminum and removal of oxide impurities in the slag. After ladle treatment, the furnace was transferred to the vacuum degassing process to ensure the complete removal of impurities. Ca in the form of CaSi was added into the vacuum degassing process to liquify the remaining impurities (in order to avoid nozzle blockage and surface defects), and finally, the furnace was transferred to the continuous casting plant to cast the steel into long bars of variable sizes. Finally, both samples were further rolled down into small diameter rods (after soaking in the furnace having a temperature ranging between 1000 and 1050 °C), i.e., GS1 was rolled to 40 mm diameter and GS2 to 25 mm.

**Table 1.** Chemical compositions of two gear steel samples (wt.%).

Grade	C	Si	Mn	Ni	Cr	*N	*P	*S	*Al	*Ca	*O	Fe
GS1	0.18	0.15	1.13	0.17	1.07	106	81	290	284	14	19	Bal.
GS2	0.21	0.25	1.31	0.028	1.26	155	68	140	407	19	20	Bal.

\*N, P, S, Al, Ca and O are in ppm.

### Analysis of Steel

Steel samples were cautiously prepared for electron probe microanalyzer (EPMA) analysis. Longitudinal sections were cut for inclusion analysis. After setting into the epoxy resin, the samples were ground up to 4000 grit size paper and slightly polished. Extensive polishing and etching can easily wash away the inclusions. A 20 × 20 mm<sup>2</sup> area of each sample was manually scanned for inclusions to ensure no inclusion was left behind.

A JXA 8200 electron probe X-ray microanalyzer (JEOL, Tokyo, Japan) with wavelength-dispersive detectors was used for microstructure and compositional analysis. Parameters employed for analysis include an accelerating voltage of 15 kV, 15 nA current, zero probe diameter, peak measuring time of 30 s, background position of ±5 µm and background measuring time of 5 s. EDS was used to identify and locate non-metallic inclusions in the steel; WDS was performed to measure their composition. Standards used for analysis were spinel (MgO-Al<sub>2</sub>O<sub>3</sub>), calcium silicate (CaSiO<sub>3</sub>), iron sulphide (FeS<sub>2</sub>), spessartine (Mn<sub>3</sub>Al<sub>2</sub>Si<sub>3</sub>O<sub>12</sub>) and hematite (Fe<sub>2</sub>O<sub>3</sub>) for Al, Mg, Ca, Si, S, Mn and Fe, respectively. The built-in ZAF correction procedure supplied with the probe was applied. Different crystals to cover the entire X-ray spectrum were used, which were lithium fluoride (LIF), pentaerythritol (PET) and thallium acid phthalate (TAP). Assuming the valence state of each element, compositions of the phases were re-calculated. The overall accuracy of the EPMA measurement of each component is within 1 wt.%.

## 3. Results and Discussion

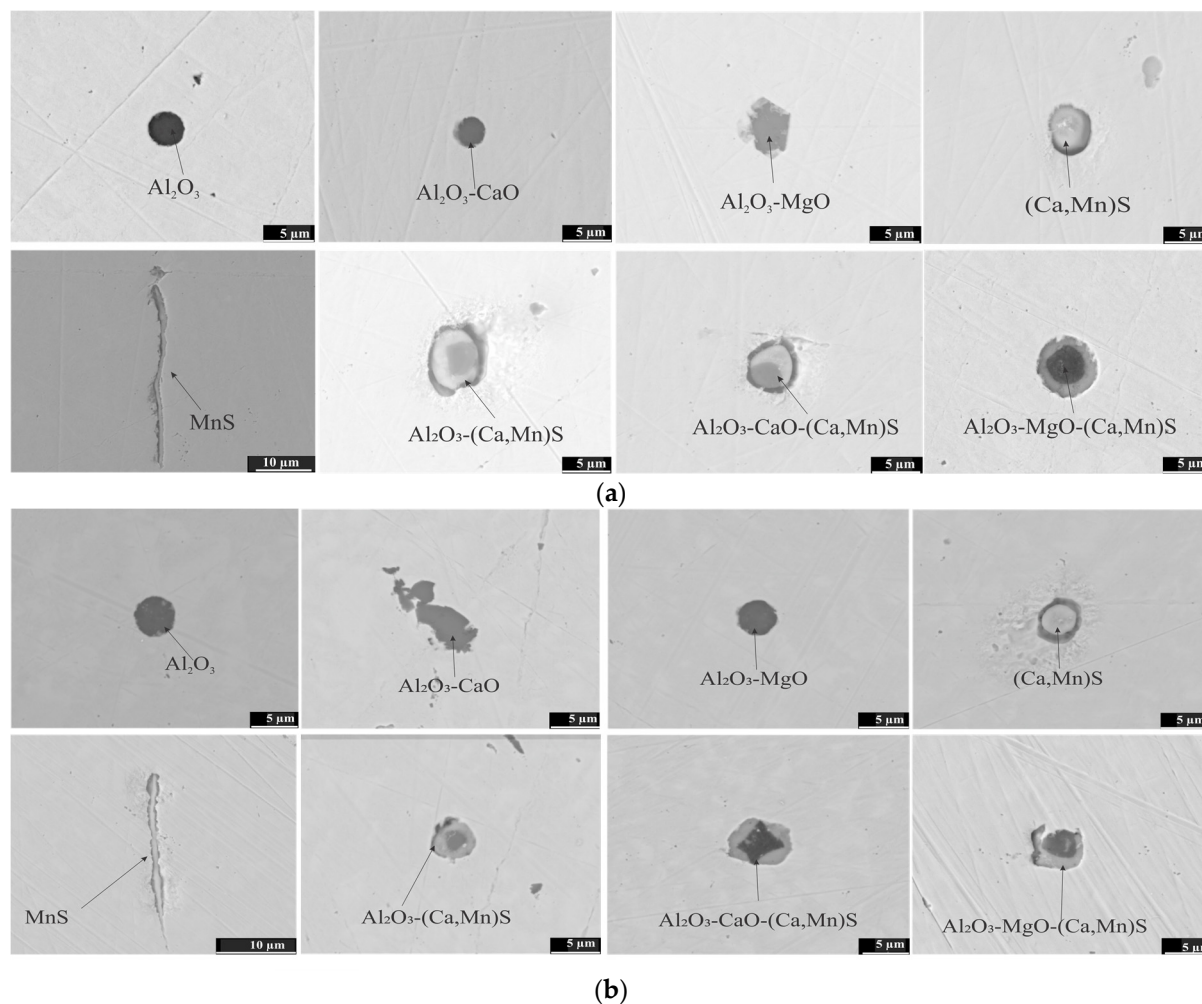
### 3.1. Morphology and Composition of Inclusions

Longitudinal sections of both GS1 and GS2 samples were scanned for a better understanding of the morphology and distribution of the inclusions. In GS1 and GS2 samples, there are approximately 300 and 370 inclusions respectively in the scanned area of 2 cm<sup>2</sup>, which was measured via EMPA. The inclusions are categorized into different groups based on their major chemical compositions and morphologies including single/dual phases and spherical/elongated sulphides. The classification of inclusions is given in Table 2, which

describes the overall composition range of oxides and sulphides in single phase and also in complex inclusions. The wt.% of alumina, silica, calcium and magnesium oxides in the inclusions along with sulphur and manganese can be easily seen. Figure 1 shows the typical inclusions in GS1 and GS2 samples based on their compositions and phases, i.e., single phase and dual phase.

**Table 2.** Classification of inclusions in both samples based on the chemical compositions and morphologies.

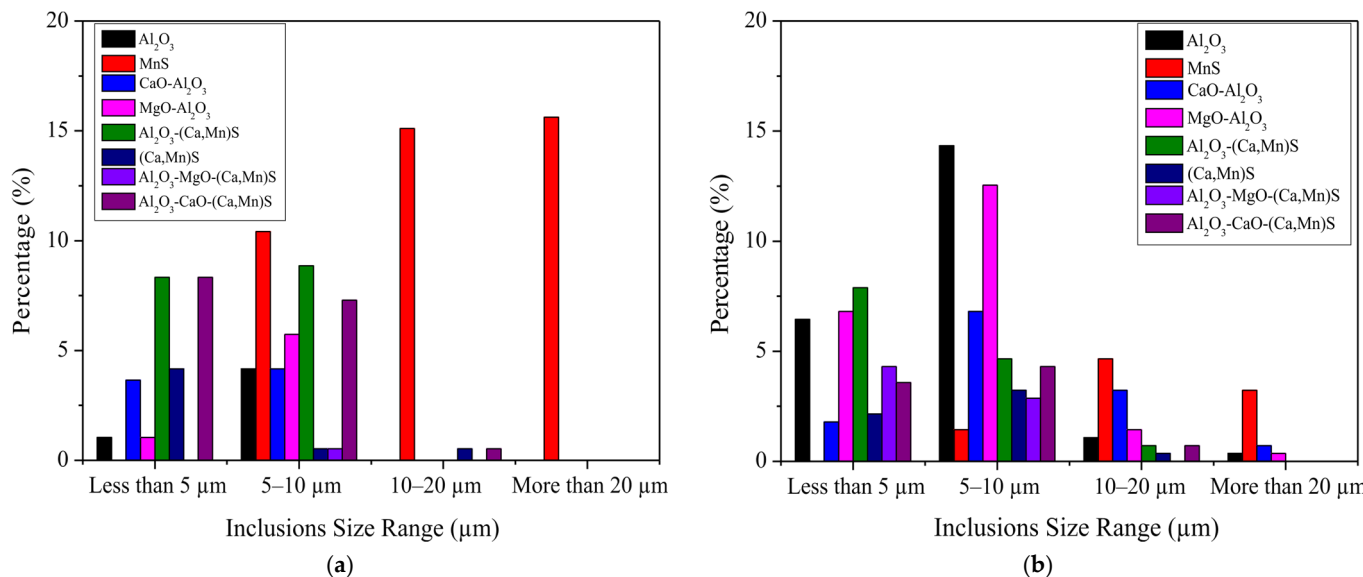
Inclusion Type	Composition Range (wt.%)						
	Al <sub>2</sub> O <sub>3</sub>	CaO	MgO	SiO <sub>2</sub>	FeO	CaS	MnS
Single Oxides	Al <sub>2</sub> O <sub>3</sub>	>80	<05	<01	<05	<05	<05
	Al <sub>2</sub> O <sub>3</sub> -CaO	>50	>40	<05	<01	<05	<05
	Al <sub>2</sub> O <sub>3</sub> -MgO	>60	<05	>30	<01	<05	<05
Sulphides	(Ca,Mn)S	<05	<05	<05	<01	<05	>45
	MnS	<05	<05	<05	<01	<05	>90
Dual Oxy-Sulphides	Al <sub>2</sub> O <sub>3</sub> -(Ca,Mn)S	>50	<05	<05	<01	<05	>20
	Al <sub>2</sub> O <sub>3</sub> -CaO-(Ca,Mn)S	>40	>20	<05	<01	<05	>15
	Al <sub>2</sub> O <sub>3</sub> -MgO-(Ca,Mn)S	>50	<05	>20	<01	<05	>15



**Figure 1.** Typical morphology and composition of inclusions in both samples. (a) GS1 sample, (b) GS2 sample.

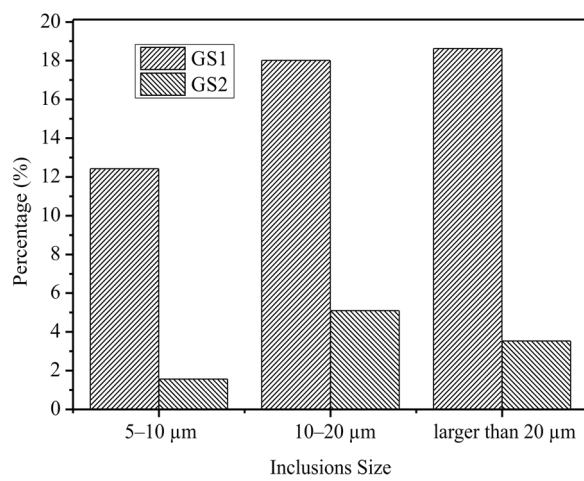
### 3.2. Number Fraction and Size Range of Inclusions

Figure 2a,b represent the detailed size and percentage distribution of individual inclusions in GS1 and GS2 samples, respectively. According to Figure 1a,b, most of the inclusions are round, while some are in irregular shapes, especially the pure MnS inclusions, which are elongated due to rolling. ImageJ (LOCI, University of Wisconsin, Madison, WI, USA) was used to measure the size of the inclusions. Most of the inclusions in the samples are regular in shape and easy to measure. For irregular inclusions morphology, the inclusion size is simply defined by measuring the longest length. Inclusions percentage is calculated by dividing the number of inclusions of each type by the total number of inclusions. In Figure 2a, there are a greater number (around 15%) of pure MnS inclusions in the range of 10–20  $\mu\text{m}$ , while around 17% of the pure MnS inclusions are larger than 20  $\mu\text{m}$ , a smaller number (only 5%) of pure alumina inclusions and a higher number of calcium-aluminates, and also complex oxy-sulphides, whereas in Figure 2b, there are around 16% pure alumina having a size greater than 5  $\mu\text{m}$ , and the spinel ( $\text{MgO}-\text{Al}_2\text{O}_3$ ) inclusions are around 14% in that size range. It is shown that the pure alumina inclusions are more in number than the complex oxides and sulphides; these inclusions are less 10  $\mu\text{m}$  in size, which is in an acceptable range for the mechanical properties of gear steels. Around 2% of the calcium aluminates are less or equal to 5  $\mu\text{m}$ , and about 8% of the calcium-aluminate inclusions are in the 5–10  $\mu\text{m}$  range. Around 9% of the total inclusions are duplex ones in which the solid solution of Ca and Mn sulphide encapsulated the alumina and spinel inclusions. Most of the inclusions are in the acceptable size range, i.e., 5–15  $\mu\text{m}$ , except the pure MnS, which was plastically deformed during rolling of the steel.



**Figure 2.** The size of different types of inclusions in the gear steels. (a) GS1 sample, (b) GS2 sample.

Figure 3 specifically represents the size comparison between pure MnS inclusions in both high and low sulphur samples, respectively. Steel with high sulphur content (GS1 sample) and only 14 ppm Ca shows a higher number of pure MnS inclusions which are elongated and also larger in size due to rolling of the steel because of the plastic (soft) nature of pure manganese sulphide, as has already been mentioned above. The inclusions of the GS2 sample with a relatively low sulphur content have a small number of pure MnS, also shown in Figure 3, but have a solid solution of  $(\text{Ca},\text{Mn})\text{S}$ . Overall, Figure 3 shows a better MnS modification result due to Ca treatment in the GS2 sample, because most of the portion of pure MnS inclusions was transformed into a solid solution of  $(\text{Ca},\text{Mn})\text{S}$ .



**Figure 3.** Pure MnS size comparison between the two samples.

#### 4. Thermodynamics of Inclusions Formation

Chemical compositions of  $\text{Al}_2\text{O}_3$ ,  $\text{Al}_2\text{O}_3\text{-MgO}$  and  $\text{Al}_2\text{O}_3\text{-CaO}$  inclusions are projected onto the  $\text{Al}_2\text{O}_3\text{-MgO-CaO}$  ternary system as shown in Figure 4a,b of both samples respectively (where M is MgO, MA is  $\text{MgO-Al}_2\text{O}_3$ , CA is  $\text{CaO-Al}_2\text{O}_3$ ,  $\text{CA}_2$  is  $\text{Ca-Al}_4\text{O}_7$ ,  $\text{CA}_6$  is  $\text{Ca-Al}_{12}\text{O}_{19}$ , C3A is  $\text{Ca}_3\text{-Al}_2\text{O}_6$  and  $\text{C}_{12}\text{A}_7$  is  $\text{Ca}_{12}\text{-Al}_{14}\text{O}_{34}$ ). The liquidus temperature of inclusions can be predicted by Figure 4. The liquidus temperature of  $\text{Al}_2\text{O}_3$ ,  $\text{Al}_2\text{O}_3$ -rich CaO, CaO-rich  $\text{Al}_2\text{O}_3$  and  $\text{Al}_2\text{O}_3\text{-MgO}$  spinel inclusions is much higher than 1600 °C, which is normally the molten steel refining temperature, while some  $\text{Al}_2\text{O}_3\text{-CaO}$  inclusions are below 1600 °C. When Al was added to molten steel as a deoxidizer,  $\text{Al}_2\text{O}_3$  inclusions were initially formed. The dissolved [Al] and [O] often reacted with traces of dissolved [Mg] or (MgO) refractory to form ( $\text{MgO-Al}_2\text{O}_3$ ) spinel inclusions. These inclusions were formed through the reduction of MgO in the slag or refractory by aluminum even though Mg was not intentionally added in the steel. Mg reacted with  $\text{Al}_2\text{O}_3$  to form  $\text{MgO-Al}_2\text{O}_3$  inclusions. The formation of spinel inclusions through a steel-slag-refractory reaction has been discussed elsewhere in detail [21,24–26]. Ca-treatment was used to transform solid spinel and solid alumina into liquid calcium aluminates [21]. However, some  $\text{Al}_2\text{O}_3$  inclusions were not properly modified by Ca treatment and formed solid  $\text{Al}_2\text{O}_3$ -rich CaO and CaO-rich  $\text{Al}_2\text{O}_3$  inclusions, which have a high liquidus temperature.

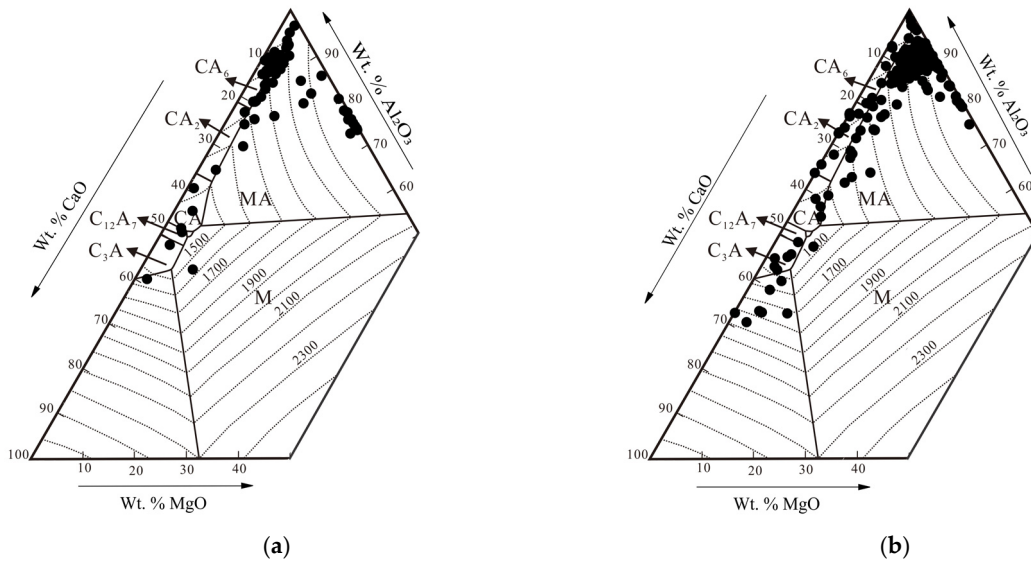


**Figure 4.** The composition distribution of  $\text{Al}_2\text{O}_3\text{-MgO-CaO}$  inclusions on the  $\text{Al}_2\text{O}_3\text{-MgO-CaO}$  phase diagram. (a) GS1 sample, (b) GS2 sample.

(Ca,Mn)S was observed to be associated with  $\text{Al}_2\text{O}_3$ -CaO inclusions to form  $\text{Al}_2\text{O}_3$ -CaO-(Ca, Mn)S oxysulphide inclusions. Kang et al. [27] measured the phase equilibria and calculated the  $\text{Al}_2\text{O}_3$ -CaO-CaS oxysulphide system using FactSage thermochemical software. To understand the solubility of CaS in the  $\text{Al}_2\text{O}_3$ -CaO at high temperature and to justify why pure CaS inclusions or CaS encapsulating oxide inclusions are not present in the present inclusions system, the  $\text{Al}_2\text{O}_3$ -CaO-CaS system was re-calculated using an updated version of the FactSage 7.3 (CRCT, Montreal, Canada and GTT Technologies, Aachen, Germany) phase diagram module using the FactOxide, FactPS, and FactMisc. databases with 1 atm pressure, and no other assumptions were considered [28], which is shown in Figure 5. The region of full-liquid phase at 1600 °C is delimited by the thinner lines on the diagram. Within the isothermal sections of 1600 °C, CaS solid precipitates in the molten steel during Ca-treatment can dissolve into liquid calcium aluminate inclusions in the primary phase fields of  $\text{Ca}_3\text{Al}_2\text{O}_6$  and  $\text{CaAl}_2\text{O}_4$ . In the CaS primary phase field, the solubility of CaS in the liquid calcium aluminate is up to 8.5 wt.%, and it decreases with increasing  $\text{Al}_2\text{O}_3$  content in the inclusions at 1600 °C. The liquid inclusions formed in GS1 and GS2 samples were calculated, which are indicated in Figure 5 as solid points. The CaS composition in liquid calcium aluminate inclusions is around 3.2 wt.%. According to Higuchi et al. the dissolved CaS will re-precipitate from the liquid  $\text{Al}_2\text{O}_3$ -CaO-CaS oxysulphide inclusions to form  $\text{Al}_2\text{O}_3$ -CaO-CaS dual phases during solidification of steel [16], but in the present case it did not happen. Precipitation of MnS on CaS at low temperature to form (Ca, Mn)S in solidified steels will be discussed in the next section.

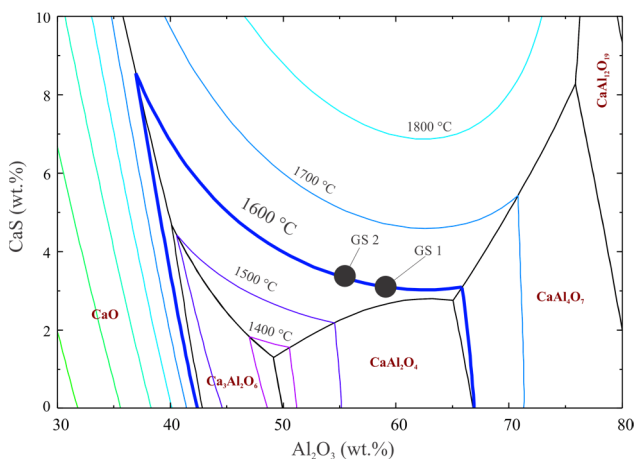


**Figure 5.** Calculated liquidus projection of  $\text{CaO}$ - $\text{Al}_2\text{O}_3$ - $\text{CaS}$  system in low  $\text{CaS}$  region.

Thermodynamics of inclusions precipitation and evolution in the equilibrium cooling of steels from 1600 °C to 1000 °C are shown in Figure 6a,b for GS1 and GS2 samples based on the chemical compositions in Table 1, respectively. Figure 6a,b show liquid calcium aluminates formed in molten GS1 and GS2 steels at 1600 °C. The ratio of  $\text{CaO}/\text{Al}_2\text{O}_3$  in the liquid oxide inclusions mainly depends on the modification extent of  $\text{Al}_2\text{O}_3$  by Ca and concentrations of Ca, Al and O in Al-killed steels. The liquid calcium aluminate inclusions transformed to the  $\text{CaAl}_2\text{O}_4$  phase at around 1600 °C, then altered from  $\text{CaAl}_4\text{O}_7$  to  $\text{CaAl}_{12}\text{O}_{19}$  and finally transformed to  $\text{Al}_2\text{O}_3$  inclusions below 1400 °C. A large number of  $\text{Al}_2\text{O}_3$  or  $\text{Al}_2\text{O}_3$ -rich inclusions were observed in the GS1 and GS2 solidified steels, as shown in their compositions in Figure 4 above, which is consistent with the thermodynamic calculations. The  $\text{Al}_2\text{O}_3$  or  $\text{Al}_2\text{O}_3$ -rich inclusions might be formed from the cooling of liquid inclusions or a deficient modification of  $\text{Al}_2\text{O}_3$  due to Ca approaching equilibrium. One thing worth noting is the amount of AlN formed in both steels; GS2 has more mass % of AlN than GS1. This is due to the fact that a greater amount of Al is used for deoxidation of steel. Nitrogen is usually added in the form of a ferroalloy for grain refinement, to prevent the austenite grain coarsening during heat treatment and to enhance the mechanical properties of the steels via grain boundary pinning through aluminum-nitride precipitates

(AlN) [29]. AlN was not detected during EPMA analysis, maybe because of the detection limit of the probe, which mostly measures inclusions larger than or equal to  $1\text{ }\mu\text{m}$ . AlN may have a sub-micron or nano size, and also the cooling rate in the ladle and during continuous casting is not at equilibrium, so maybe that is why AlN was unable to be detected by the probe despite the prediction during thermodynamic calculations.

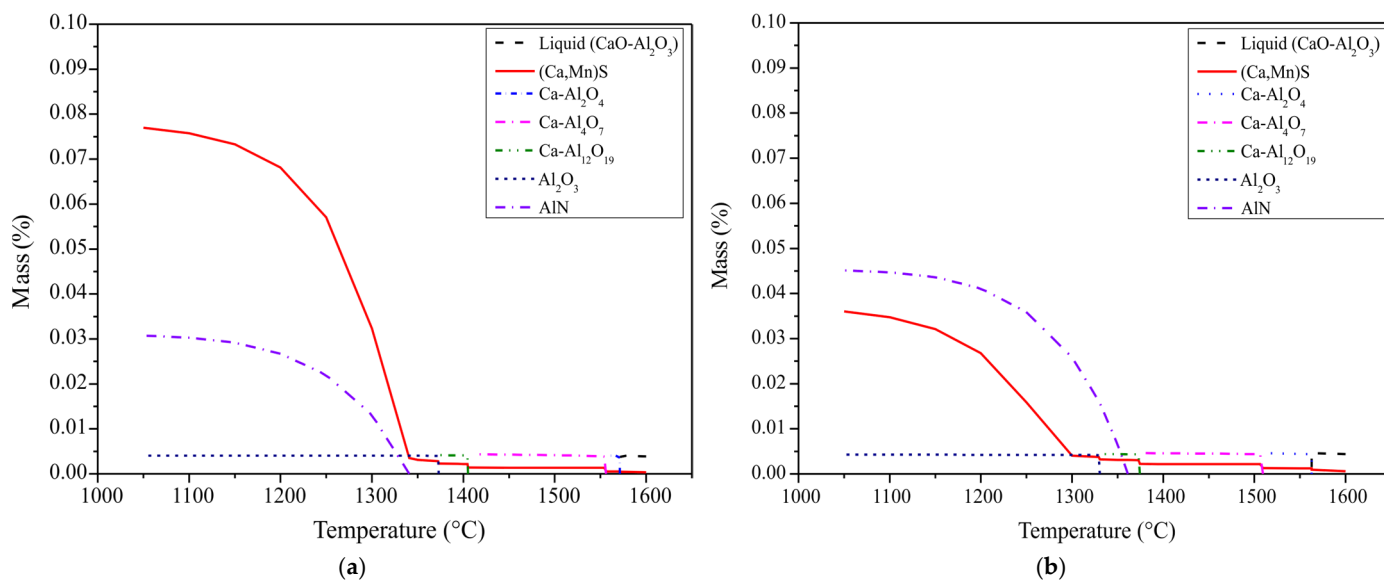


**Figure 6.** Equilibrium precipitation of inclusions and evolution during steel solidification. (a) GS1 sample, (b) GS2 sample.

The variation of CaS and MnS components in the (Ca, Mn)S solid solution in equilibrium solidification in both samples is specifically shown in Figure 7. According to FactSage calculations, nearly pure CaS precipitated in molten Ca-treated Al-killed GS1 and GS2 steels at  $1600\text{ }^{\circ}\text{C}$ . The formation of solid CaS is usually caused by excessive sulphur and calcium in liquid steel. At steel melting temperature, both Ca and S have high activities and the amount of CaS generated in both samples is more than 90%. In GS1, with the decrease in temperature, this amount decreases until it reaches the balance with MnS at around  $1330\text{ }^{\circ}\text{C}$ , and after that, MnS begins to grow at the expense of CaS and reaches more than 90% at around  $1000\text{ }^{\circ}\text{C}$ , whereas CaS is only less than 10% at that temperature. On the other hand, in GS2, with the decrease in temperature the amount of CaS decreases until  $1270\text{ }^{\circ}\text{C}$ . The analysis of samples showed different results in the case of CaS inclusions, as proved by Figure 5. Individual or complex oxy-CaS inclusions were not observed during EPMA analysis because CaS was dissolved in the CaO-Al<sub>2</sub>O<sub>3</sub> and did not solidify as CaO-Al<sub>2</sub>O<sub>3</sub>-CaS. Detailed mechanism of inclusions evolution during solidification can be seen in Figure 8. Decrease in CaS in the GS2 sample at a lower temperature can provide the complete casting of several heats with no nozzle blockage and a lower amount of MnS generated.

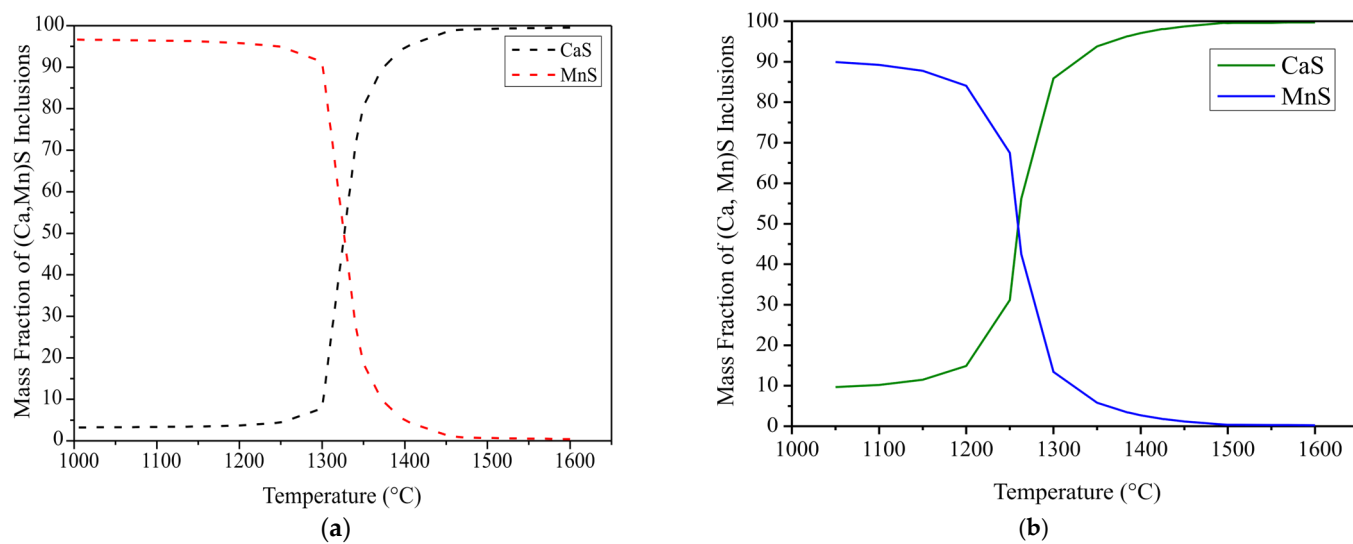


**Figure 7.** Mass percentage of CaS and MnS in the solid solution of (Ca,Mn)S. (a) GS1 sample, (b) GS2 Sample.

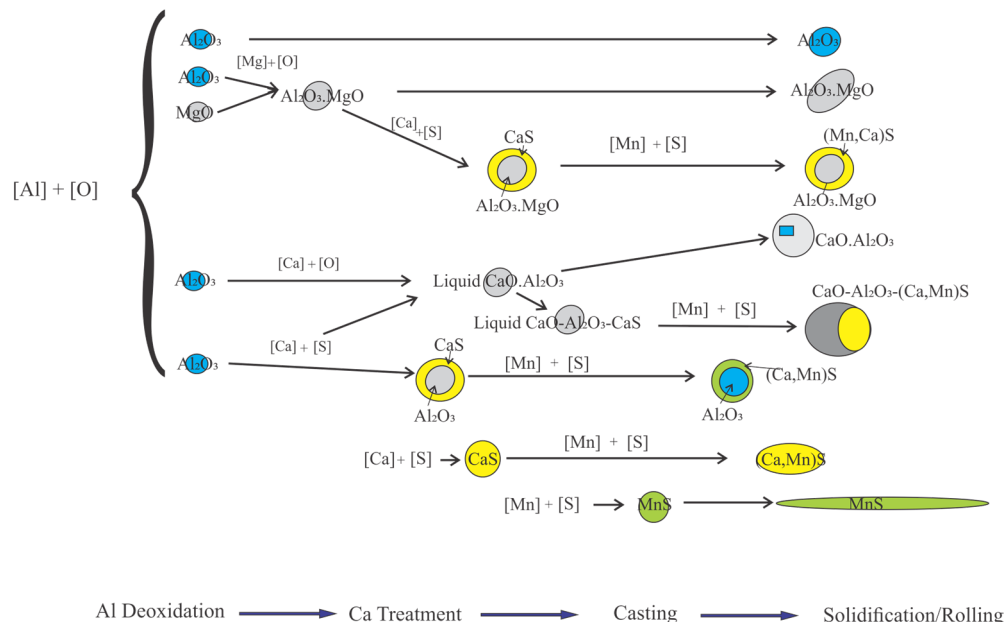


**Figure 8.** The schematic diagram of inclusions formation at the different stages of Al deoxidation, Ca treatment and solidification.

## 5. Formation Mechanism of Inclusions

The reactions during modification of alumina inclusions by calcium can be divided into the following kinetic steps:

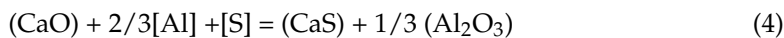
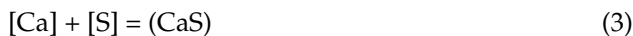
1. Ca injection into the ladle, which immediately melts the Ca, because its melting point is much lower than the melting temperature of steel, followed by the dissolution of calcium from the gas bubbles-steel interface to the bulk of the steel and finally transfer of the dissolved calcium from the bulk steel to the steel-inclusion interface:



2. Diffusion of calcium from the steel-inclusion interface into the alumina core followed by chemical reaction of the calcium with alumina:



3. The sulphur content varies in both samples, consequently the extent of CaS formation changes. Ca can react with sulphur in two ways:



In the above equations, square brackets denote an element dissolved in molten steel, and round brackets indicate the compounds in the inclusions. Before the calcium-alloy wire injection, mainly  $\text{Al}_2\text{O}_3$  was produced due to the Al deoxidation of liquid steel. During the calcium treatment, the injection of Ca will lead to a severe splashing of liquid steel due to the high vapor pressure of Ca, and the added  $[\text{Ca}]$  reacts with  $[\text{O}]$  and  $\text{Al}_2\text{O}_3$  inclusions to transform solid  $\text{Al}_2\text{O}_3$  to liquid calcium aluminate inclusions. Some semi-solid  $\text{Al}_2\text{O}_3$ -rich core-shell inclusions might be partially modified due to kinetic diffusion of  $[\text{Ca}]$  controlling limitation [30–32]. When the  $[\text{S}]$  content is higher than the critical value for the precipitation of CaS, the  $\text{CaO}$  in the liquid inclusions reacts with sulphur  $[\text{S}]$  and aluminum  $[\text{Al}]$  in the molten steel. Therefore, the composition of the inclusions in the core is transformed to a  $\text{MgO}\cdot\text{Al}_2\text{O}_3$ -rich system (close to spinel), and a CaS shell is formed. On the other hand, when the  $[\text{S}]$  content is lower than the critical value for the precipitation of CaS, liquid inclusions are formed [21]. The solubility of  $[\text{Mn}]$  and  $[\text{S}]$  decreases during the solidification of steels. Segregation of  $[\text{Mn}]$  and  $[\text{S}]$  takes the primary inclusions as the heterogeneous nucleation sites for MnS precipitation, then reacts with primary CaS wrapping on the oxides to form  $(\text{Ca},\text{Mn})\text{S}$  solid solution [32–35]. A schematic diagram of inclusions formation is demonstrated in Figure 8 and can be visualized via SEM-EDS analysis as shown in Figure 9. Figure 9 with EDS scanning explains the formation of a crescent shaped  $(\text{Ca},\text{Mn})\text{S}$  layer surrounding the spinels and in the other image it shows the oval shape  $(\text{Ca},\text{Mn})\text{S}$  associated with the spinels.

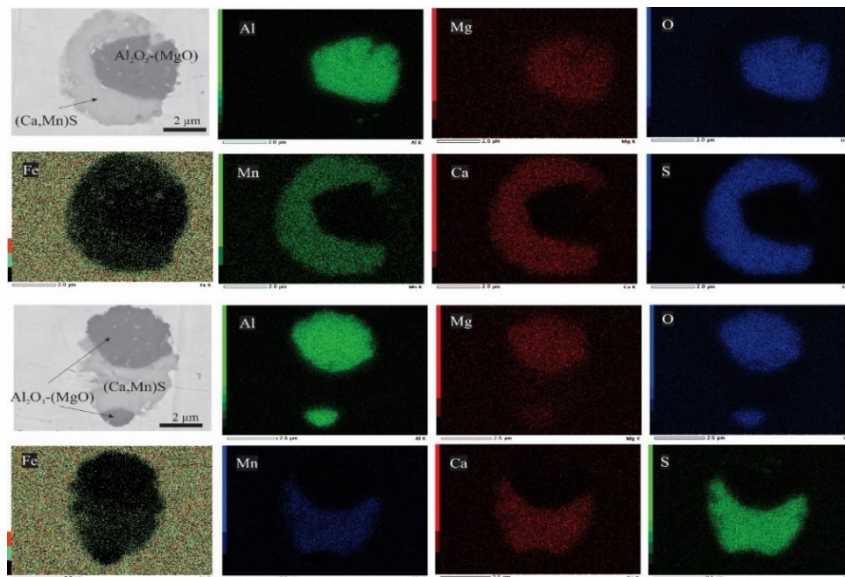


**Figure 9.** Duplex inclusions formed by  $(\text{Ca},\text{Mn})\text{S}$  precipitated on and collided with  $\text{Al}_2\text{O}_3\text{-MgO}$  inclusions.

The stable inclusions which can be formed based on the compositions of GS1 and GS2 in Table 1 by varying  $[\text{Al}]$  and  $[\text{Ca}]$  were calculated using FactSage 7.3 software with a phase diagram module with 1 atm pressure (FactOxide, FactPS and FactMisc. databases) to understand the controlling of inclusions. Figure 10 shows the stability diagram of the inclusions formed in the Fe-C-Si-Mn-Cr-S-O-Al-Ca systems at 1600 °C. The compositions of GS1 and GS2 are located close to the boundary of  $\text{CaS} + \text{liquid}$  and totally liquid inclusions region, which indicates the amount of CaS is relatively small. The small amount of CaS might not cause the problem of nozzle clogging in one heat casting but could block the

nozzle by accumulating in the nozzle after several castings in practice. The liquid inclusions region is the target for successful modification of inclusions but not the whole region is the target because either decrease in [Al] content less than 150 ppm will yield other oxides, specially FeO and MnO, or decrease in [Ca] content less than 10 ppm will not completely modify the alumina inclusions but form (high temperature stable)  $\text{CaAl}_4\text{O}_7$  inclusions which may create problems during casting. The modification window of Ca-treatment is quite narrow and should be controlled precisely.

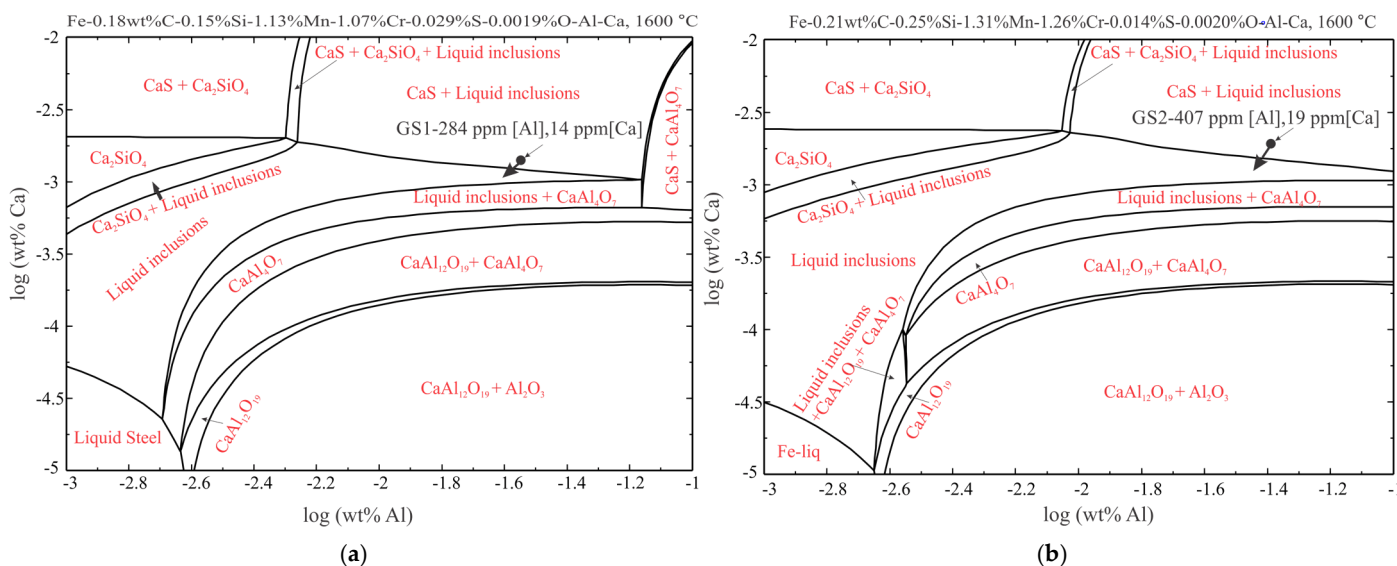


**Figure 10.** Stability diagram of inclusions formed in the Fe-C-Si-Mn-Cr-S-O-Al-Ca system at 1600 °C. (a) GS1 sample, (b) GS2 sample.

## 6. Conclusions

In the present study two gear steel samples with different sulphur and calcium contents were analyzed using an electron probe micro-analysis (EPMA) technique coupled with thermodynamic studies. The main findings are:

1. A significant number of pure MnS inclusions were observed in high sulphur steel as compared to low sulphur steel. Duplex inclusions and some spinel cores encapsulated by sulphides were also observed. (Ca,Mn)S encapsulated most of the oxide inclusions in both samples and no transient ( $\text{CaO}-\text{Al}_2\text{O}_3-\text{CaS}$ ) inclusions were precipitated in the solidified steel despite it having a high sulphur content, i.e., 290 ppm and 140 ppm, respectively.
2. Calcium aluminates with a low melting temperature were formed in low sulphur steel, which is considered desirable for continuous casting. The main factors that influence the size, morphology and distribution of inclusions are the Al, S, O and Ca contents in the steel and its temperature.
3. The thermodynamic stability diagram of inclusions in Fe-C-Si-Mn-Cr-S-O-Al-Ca systems at 1600 °C agrees well with the inclusions of both sulphur-level Ca-treated samples, which shows inclusions can be completely modified into liquid ones by decreasing the content of Ca up to 10 ppm. Further decreasing the Ca content will result in incomplete modification of oxides and sulphides, and the formation of (high temperature stable) aluminates (CA2) will occur.

**Author Contributions:** Conceptualization, S.L. and H.A.; methodology, S.Z., Y.X. and Z.H.; software, H.A.; validation, S.L., X.M. and B.Z.; formal analysis, S.L.; investigation, H.A.; resources, H.A.; data curation, S.L.; writing—original draft preparation, H.A.; writing—review and editing, X.M.; supervision, X.M.; project administration, B.Z.; funding acquisition, B.Z. All authors have read and agreed to the published version of the manuscript.

**Funding:** This research and APC were funded by the Australian Government through the Australian Research Council Research Hub for Computational Particle Technology, grant number IH140100035.

**Data Availability Statement:** The manuscript does not contain any data that has already been reported or archived elsewhere.

**Acknowledgments:** This research was supported by the Australian Government through the Australian Research Council Research Hub for Computational Particle Technology (IH140100035) and Baosteel through Baosteel-Australia Joint Research and Development Centre. The Australian Microscopy & Microanalysis Research Facility is acknowledged for providing characterization facilities. Technical support for the EPMA facility from Ron Rasch and Ying Yu of the Centre for Microscopy and Microanalysis at the University of Queensland is gratefully acknowledged.

**Conflicts of Interest:** The authors declare no conflict of interest.

## References

1. Tönshoff, H.; Stanske, C. High productivity machining: Materials and processes. In Proceedings of International Conference on High Productivity Machining, Materials and Processing, New Orleans, LA, USA, 7–9 May 1985; pp. 7–9.
2. Kirsch-Racine, A.; Bomont-Arzur, A.; Confente, M. Calcium treatment of medium carbon steel grades for machinability enhancement: From the theory to industrial practice. *Metall. Res. Technol.* **2007**, *104*, 591–597. [[CrossRef](#)]
3. Vasconcellos da Costa e Silva, A.L. The effects of non-metallic inclusions on properties relevant to the performance of steel in structural and mechanical applications. *J. Mater. Res. Technol.* **2019**, *8*, 2408–2422. [[CrossRef](#)]
4. Maciejewski, J. The Effects of Sulfide Inclusions on Mechanical Properties and Failures of Steel Components. *J. Fail. Anal. Prev.* **2015**, *15*, 169–178. [[CrossRef](#)]
5. Cyril, N.; Fatemi, A. Experimental evaluation and modeling of sulfur content and anisotropy of sulfide inclusions on fatigue behavior of steels. *Int. J. Fatigue* **2009**, *31*, 526–537. [[CrossRef](#)]
6. Murty, Y.; Morral, J.; Kattamis, T.; Mehrabian, R. Initial coarsening of manganese sulfide inclusions in rolled steel during homogenization. *Metall. Trans. A* **1975**, *6*, 2031–2035. [[CrossRef](#)]
7. Ånmark, N.; Karasev, A.; Jönsson, P.G. The Effect of Different Non-Metallic Inclusions on the Machinability of Steels. *Materials* **2015**, *8*, 751–783. [[CrossRef](#)]
8. Li, M.-L.; Wang, F.-M.; Li, C.-R.; Yang, Z.-B.; Meng, Q.-Y.; Tao, S.-F. Effects of cooling rate and Al on MnS formation in medium-carbon non-quenched and tempered steels. *Int. J. Miner. Metall. Mater.* **2015**, *22*, 589–597. [[CrossRef](#)]
9. Huang, F.; Su, Y.F.; Kuo, J.-C. Microstructure and Deformation Characteristics of MnS in 1215MS Steel at 1050 °C. *Int. Conf. Min. Mater. Metall. Eng.* **2017**, *191*, 1333–1345.
10. Liu, Y.; Zhang, L. Relationship between Dissolved Calcium and Total Calcium in Al-Killed Steels after Calcium Treatment. *Met. Mater. Trans. A* **2018**, *49*, 1624–1631. [[CrossRef](#)]
11. Jeon, S.-H.; Kim, S.-T.; Lee, J.-S.; Lee, I.-S.; Park, Y.-S. Effects of Sulfur Addition on the Formation of Inclusions and the Corrosion Behavior of Super Duplex Stainless Steels in Chloride Solutions of Different pH. *Mater. Trans.* **2012**, *53*, 1617–1626. [[CrossRef](#)]
12. Xin, X.; Yang, J.; Wang, Y.; Wang, R.; Wang, W.; Zheng, H.; Hu, H. Effects of Al content on non-metallic inclusion evolution in Fe-16Mn-x Al-0.6 C high Mn TWIP steel. *Ironmak. Steelmak.* **2016**, *43*, 234–242. [[CrossRef](#)]
13. Guo, Y.-T.; He, S.-P.; Chen, G.-J.; Wang, Q. Thermodynamics of Complex Sulfide Inclusion Formation in Ca-Treated Al-Killed Structural Steel. *Met. Mater. Trans. A* **2016**, *47*, 2549–2557. [[CrossRef](#)]
14. Diederichs, R.; Bleck, W. Modelling of Manganese Sulphide Formation during Solidification, Part I: Description of MnS Formation Parameters. *Steel Res. Int.* **2006**, *77*, 202–209. [[CrossRef](#)]
15. Blais, C.; L’Espérance, G.; LeHuy, H.; Forget, C. Development of an integrated method for fully characterizing multi-phase inclusions and its application to calcium-treated steels. *Mater. Charact.* **1997**, *38*, 25–37. [[CrossRef](#)]
16. Higuchi, Y.; Numata, M.; Fukagawa, S.; Shinme, K. Inclusion Modification by Calcium Treatment. *ISIJ Int.* **1996**, *36*, S151–S154. [[CrossRef](#)]
17. Tiekkink, W.; Santillana, B.; Kooter, R.; Menzonides, F.; Deo, B.; Boom, R. Calcium: Toy, tool or trouble. *AIST Trans.* **2008**, *5*, 395–403.
18. Verma, N.; Pistorius, P.; Fruehan, R.J.; Potter, M.; Lind, M.; Story, S. Transient Inclusion Evolution during Modification of Alumina Inclusions by Calcium in Liquid Steel: Part, I. Background, Experimental Techniques and Analysis Methods. *Met. Mater. Trans. A* **2011**, *42*, 711–719. [[CrossRef](#)]
19. Verma, N.; Pistorius, P.C.; Fruehan, R.J.; Potter, M.; Lind, M.; Story, S.R. Transient inclusion evolution during modification of alumina inclusions by calcium in liquid steel: Part II. Results and discussion. *Metall. Mater. Trans. B* **2011**, *42*, 720–729. [[CrossRef](#)]

20. Wang, Y.; Sridhar, S.; Valdez, M. Formation of CaS on  $\text{Al}_2\text{O}_3$ -CaO inclusions during solidification of steels. *Met. Mater. Trans. A* **2002**, *33*, 625–632. [[CrossRef](#)]
21. Shin, J.H.; Park, J.H. Formation Mechanism of Oxide-Sulfide Complex Inclusions in High-Sulfur-Containing Steel Melts. *Met. Mater. Trans. A* **2017**, *49*, 311–324. [[CrossRef](#)]
22. Wakoh, M.; Sawai, T.; Mizoguchi, S. Effect of S Content on the MnS Precipitation in Steel with Oxide Nuclei. *ISIJ Int.* **1996**, *36*, 1014–1021. [[CrossRef](#)]
23. Fukaya, H.; Miki, T. Phase Equilibrium between  $\text{CaO}\cdot\text{Al}_2\text{O}_3$  Saturated Molten  $\text{CaO}-\text{Al}_2\text{O}_3-\text{MnO}$  and (Ca, Mn) S Solid Solution. *ISIJ Int.* **2011**, *51*, 2007–2011. [[CrossRef](#)]
24. Park, J.H.; Todoroki, H. Control of  $\text{MgO}\cdot\text{Al}_2\text{O}_3$  spinel inclusions in stainless steels. *ISIJ Int.* **2010**, *50*, 1333–1346. [[CrossRef](#)]
25. Harada, A.; Matsui, A.; Nabeshima, S.; Kikuchi, N.; Miki, Y. Effect of slag composition on  $\text{MgO}\cdot\text{Al}_2\text{O}_3$  spinel-type inclusions in molten steel. *ISIJ Int.* **2017**, *57*, 1546–1552. [[CrossRef](#)]
26. Shin, J.H.; Park, J.H. Modification of inclusions in molten steel by Mg-Ca transfer from top slag: Experimental confirmation of the ‘refractory-slag-metal-inclusion (ReSMI)’ multiphase reaction model. *Metall. Mater. Trans. B* **2017**, *48*, 2820–2825. [[CrossRef](#)]
27. Piao, R.; Lee, H.-G.; Kang, Y.-B. Experimental investigation of phase equilibria and thermodynamic modeling of the  $\text{CaO}-\text{Al}_2\text{O}_3-\text{CaS}$  and the  $\text{CaO}-\text{SiO}_2-\text{CaS}$  oxysulfide systems. *Acta Mater.* **2013**, *61*, 683–696. [[CrossRef](#)]
28. Bale, C.; Chartrand, P.; Degterov, S.; Eriksson, G.; Hack, K.; Ben Mahfoud, R.; Melançon, J.; Pelton, A.; Petersen, S. FactSage thermochemical software and databases. *Calphad* **2002**, *26*, 189–228. [[CrossRef](#)]
29. Dogan, Ö.N.; Michal, G.; Kwon, H.-W. Pinning of austenite grain boundaries by AlN precipitates and abnormal grain growth. *Metall. Trans. A* **1992**, *23*, 2121–2129. [[CrossRef](#)]
30. Kor, J.; Glaws, P. The Making, Shaping and Treating of Steel. Ladle refining and vacuum degassing. *Pittsburg* **1998**, *10*, 661–692.
31. Tabatabaei, Y.; Coley, K.S.; Irons, G.A.; Sun, S. Model of inclusion evolution during calcium treatment in the ladle furnace. *Metall. Mater. Trans. B* **2018**, *49*, 2022–2037. [[CrossRef](#)]
32. Liu, Y.; Zhang, L.; Zhang, Y.; Duan, H.; Ren, Y.; Yang, W. Effect of Sulfur in Steel on Transient Evolution of Inclusions During Calcium Treatment. *Met. Mater. Trans. A* **2018**, *49*, 610–626. [[CrossRef](#)]
33. Yang, W.; Zhang, L.; Wang, X.; Ren, Y.; Liu, X.; Shan, Q. Characteristics of Inclusions in Low Carbon Al-Killed Steel during Ladle Furnace Refining and Calcium Treatment. *ISIJ Int.* **2013**, *53*, 1401–1410. [[CrossRef](#)]
34. Zhao, D.; Li, H.; Bao, C.; Yang, J. Inclusion Evolution during Modification of Alumina Inclusions by Calcium in Liquid Steel and Deformation during Hot Rolling Process. *ISIJ Int.* **2015**, *55*, 2115–2124. [[CrossRef](#)]
35. Gollapalli, V.; Rao, M.V.; Karamched, P.S.; Borra, C.R.; Roy, G.G.; Srirangam, P. Modification of oxide inclusions in calcium-treated Al-killed high sulphur steels. *Ironmak. Steelmak.* **2019**, *46*, 663–670. [[CrossRef](#)]